

# THERMAL APPLICATIONS OF OPEN CELL METAL FOAMS

**Burhan Ozmat, Bryan Leyda and Burt Benson**

ERG, Materials and Aerospace Corporation  
900 Stanford Avenue, Oakland, CA 94608

**Abstract:** The key structural and thermo-physical properties of Reticulated Metal Foams (RMF) are reviewed. Analytical expressions relating such properties to basic structural parameters are developed through mathematical modeling and experimental studies. Conductive and convective aspects of thermal energy transfer through RMF based heat exchangers are reviewed. Mathematical model is developed which calculates maximum thermal performance for such heat exchangers. Results of experimental and Finite Element Analysis predicting thermal performance of test module using a thermal base plate, a power device and RMF heat exchanger and off the shelf external cold plate compared. The superior performance of RMF based heat exchangers are shown.

## **1) Introduction:**

It is being realized that the thermal aspects of many advancing technologies are in the critical path limiting the performance, size and the cost future products. The Reticulated Metal Foams (RMF), see Figure 1 for their physical structure, developed for structural application more than two decades ago are now becoming effective solutions to the many thermal management problems. The RMF offer a cost effective and ultra high performance thermal management technology that can be integrated with advanced high performance electronic, photonic devices and with many other challenging applications.

The metal foam based thermal technology is generic, flexible and scaleable. It is generic in terms of its compatibility with the cooling media ranging from DI water, inert fluorocarbons, and jet fuel to air He or Ar. It is flexible in terms of its compatibility with various semiconductor devices and substrates such as Si, GaAs, and SiC, SiN not excluding many other ceramic metallic or composite materials. The metal foam based thermal technology is scaleable both in size and performance so that it could be applied to not only discrete devices but also to Hybrid Multi Chip Modules (HMCM) integrating photonic and electronic devices, and also to double sided Printed Wiring Boards (PWB) with constraining cores. The performance of the metal foam based advanced heat exchangers is also scalable along with its cost to address a wide range of both military and commercial applications. In a broader sense, it takes advantage of the materials and technologies developed under DoD contracts, and create synergism by increasing the value of R&D spending to the US economy.

## **2) Summary:**

The most significant benefits of the proposed technology include; elimination of as many thermal interfaces between the source of heat dissipation and the heat sink i.e. the ambient viewed as the circulating coolant in an open loop (air) or closed loop system (liquid or gas). The elimination of thermal interfaces will have a significant impact on the

junction to ambient thermal resistance ( $R_{ja}$ ) of the system. The advanced thermal management technology also improves the apparent convective energy transfer  $h.A.\Delta T$  by improving the effective values of each and every term scaling the convective heat flux. These terms are: film coefficient  $h$ , heat transfer area  $A$ , and the temperature difference  $\Delta T$ .

At a higher level observation, significant improvements will be seen in the volume, weight, performance and the life cycle cost of, among others, electronic, photonic or hybrid systems.

Systems integrating high performance power devices into megawatt level power converters for Navy ships and submarines, More Electric Aircraft (MEA), power utilities and transportation vehicles such as trains, streetcars and electric vehicles are among the most suitable applications. Pump modules for solid state high-power one or two dimensional laser arrays with power dissipation levels up to  $500W/cm^2$  [1,2] military and commercial Transmit /Receive (T/R) communication, data transfer modules are also among the potential near term application platforms.

For the electro-optic systems where global or local thermal displacements may give rise to alignment related optical losses, and where detectors and lasers need to operate in a limited range of wave lengths (or temperature) a self regulating thermal management systems with built in temperature control capability may offer significant advantages. The metal foam based thermal management technology may be set to regulate temperatures in a narrow range ( $\Delta T \sim 10^\circ C$  to  $20^\circ C$ ) within a wide interval from approximately  $30^\circ C$  to  $100^\circ C$ .

The advanced Integral RMF based Heat Exchanger HX technology offers significant cost, volume, weight and performance advantages relative to the state-of-art alternate approaches. For example, the state of the art thermal management technology for high performance power modules relies on heat spreading through a relatively thick ( $\sim 0.32$  cm) Cu heat spreader thermal base which is thermally coupled to a liquid or air cooled heat sink through a thermally conducting organic compound. This approach increases both the volume and the weight of the power modules, derates the capabilities of advanced power devices due to the limited heat flux. Therefore, the current approach forces us to increase the number of devices to be used. It also increases the cost of materials, which is related to the module size, and limits the reliability of the thermal and electrical interfaces between Si and Cu due to the large Coefficient of Thermal Expansion (CTE) mismatch. Another state-of-the art approach uses heat pipes to remove the heat from modules to an external heat exchanger. This approach too relies on soft interfaces to thermally couple the heat pipes to modules, which increases the thermal resistance significantly. In addition, heat pipes add cost, volume and weight to the system.

Another alternate approach is to utilize micro channels mechanically or chemically formed in the back face of the semiconductor substrate. The microchannel approach reduces the junction to case  $R_{jc}$  significantly. However, the flow resistance and structural reliability of high aspect ratio channel cut into inherently brittle semiconductor substrate are among the major drawbacks of the approach. Integrating a suitable leak tight cover and inlet and outlet manifold structures further increases the complexity of the system. Such formed microchannel also adversely affect the device yields and reliability.

In summary, RMF based HX minimizing the number of thermal interfaces, improve the effective film coefficients, increasing the effective surface area for heat transfer. It can be controlling and/or reducing coolant temperatures by use of phase change materials encapsulated by thin micro spheres. It may significantly reduce the instabilities inherent in the nucleate boiling heat transfer [3]. It also offers structural compatibility with semiconductor devices and substrates so that direct attachment becomes possible.

### 3) Description of the RMF based HX Technology

The integral compact heat exchanger eliminates the highly resistive external thermal interfaces such as thermal pads, thermal pastes or thermal epoxies used to couple the electronic and photonic HMCN with external air cooled or liquid cooled heat sinks [4]. In addition, the integral compact heat exchanger may offer a large surface area and improved film coefficients help increase the thermal performance significantly

The HX consists of a reticulated foam made out of a high thermal conductivity material such as Al, Cu, Ag, SiC or graphite. This RMF can be metallurgically bonded by soldering or brazing techniques to high performance electronic, opto-electronic devices or to the insulating thermal bases of MCM/HMCN for maximum performance.

Configuration of the metal foams that are commercially available, have a pore density of 5, 10, 20 and 30 pore per inch (ppi). They are approximately at 8% theoretical density and made out of, 1100 Al, C102 Cu or Ag. The initial macro-structure of the foam is considered isotropic with randomly oriented ligaments. In the micro scale the foam structure consists of cells shaped as 14 sided polygons (dodecahedron). The important parameters of the foam are; thermal conductivity, heat transfer surface area and its mechanical compliance.

#### 3.1) Structure of reticulated metal foams

In the as fabricated state, the isotropic RMF consists of randomly oriented polygon shaped cells that could be approximated by dodecahedron (Figure 1) [5,6,7]

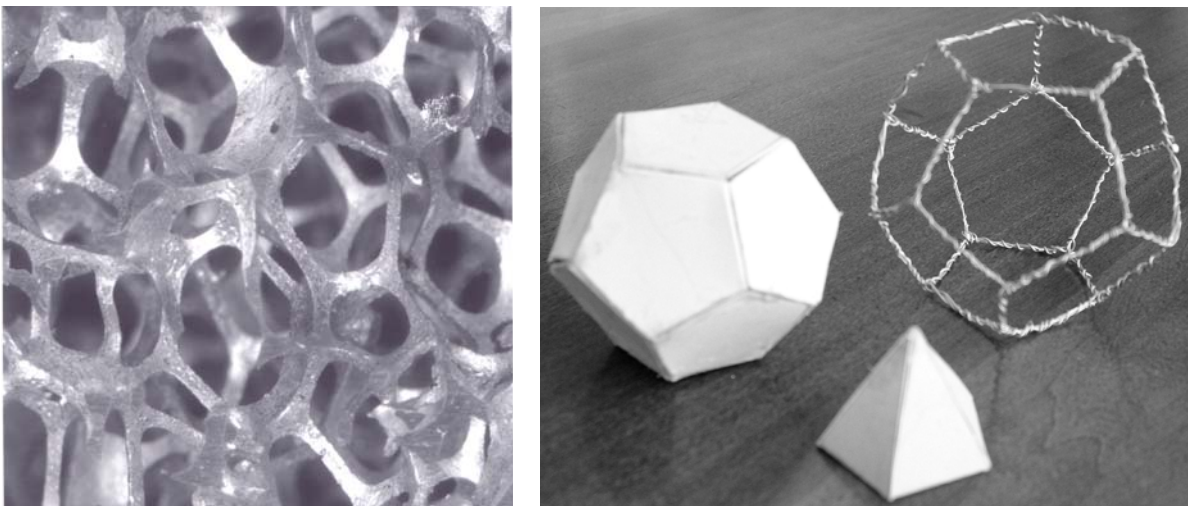


Figure 1. Structure of metal foam and dodecahedron having 12 pentagon shaped facets.

Notice that a dodecahedron may be divided into twelve identical pyramids having a pentagon shaped base. When assembled the vertex of these pyramids meet at the centroid of the dodecahedron.

Some geometric characteristics of dodecahedron are related to the physical structure of the reticulated metal foams, such as ligament size, surface area, cell density, and relative density. The average height and the volume of the dodecahedron will be reviewed below.

The apex and base angles of the five isosceles triangles of the pentagon shaped faces are;

$$2\theta = 360^\circ / 5 = 72^\circ, \text{ and } \phi = 54^\circ \quad (1)$$

respectively. The angle between the base of the dodecahedron and the plane of the adjacent pentagon face  $\phi$ , the side  $s$  and the height  $h_{pt}$  of a face, and the height of the pyramid (half the minimum height of the dodecahedron)  $h_{pd} = 1/2 h_{d,min}$  are given by the equations (2,3 and 4).

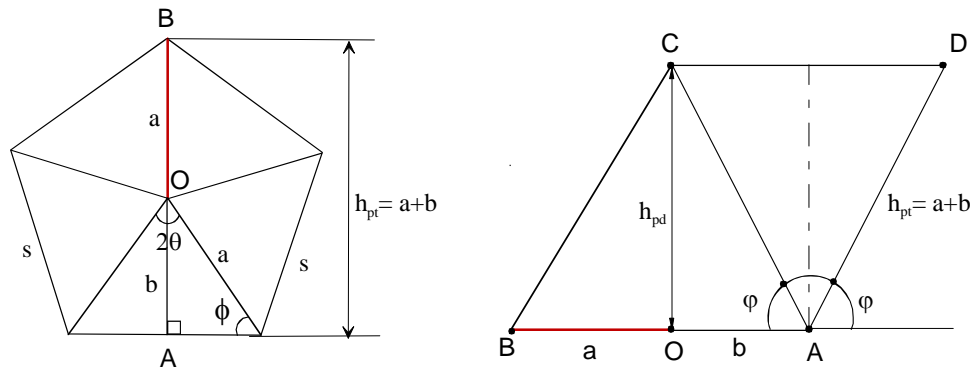


Figure 2. Geometric features of a dodecahedron

$$\phi = \text{Cos}^{-1}\left(\frac{\text{Cos}\theta}{1 + \text{Cos}\theta}\right), \text{ and } \phi \approx 63.4^\circ \quad (2)$$

$$h_{pt} = a + b = \frac{s}{2} \cdot \left(\frac{1 + \text{cos}\theta}{\text{Sin}\theta}\right) \quad (3)$$

and, 
$$h_{d,min} = (h_{pt} + s) \cdot \text{Sin}\phi = \left[\left(\frac{1 + \text{Cos}\theta}{2\text{Sin}\theta}\right) + 1\right] \cdot \text{Sin}\phi \cdot s \quad (4)$$

The maximum height or the length of the longest diagonal dimension of a dodecahedron is given by the equations (5,6 and 7) below, where  $\Delta z$ ,  $h_o$  and  $h_{d,max}$  form a right triangle.

$$\Delta z = (h_{pt} - s) \cdot \sin \varphi \quad (5)$$

$$h_o = h_{pt}(1 + \cos \varphi) + s \cdot \cos \varphi \quad (6)$$

$$h_{d,max} = \sqrt{\Delta z^2 + h_o^2} \quad (7)$$

The average dimension of a dodecahedron may be related to the cell density  $\alpha$  of a metal foam given as pore per inch (ppi) by equation (8). The maximum, the minimum and the arithmetic mean of these two measures of a dodecahedron are related to the side “s” by (9).

$$\frac{1}{\alpha} \approx \left( \frac{h_{d,max} + h_{d,min}}{2} \right) \approx 2.5 s \quad (8)$$

$$h_{d,max} = 2.7 s, \quad h_{d,min} = 2.27 s, \quad h_{d,avg} \approx 2.5 s \quad (9)$$

The volume,  $V_d$  of a dodecahedron is 12 times the volume of its pyramids with pentagon shaped base,  $A_b$  which consists of 5 isosceles triangles as shown in Figure 2 above.

$$A_b = \left( \frac{5}{2} \right) \frac{1}{\tan \theta} s^2 \quad (10)$$

$$h_{pt} = \frac{h_{d,min}}{2}, \quad \text{and} \quad V_d = 4 \cdot (A_b \cdot h_{pt}) = \frac{15 + 7\sqrt{5}}{4} s^3 \approx 7.66 \cdot s^3 \quad (11)$$

### 3.2) Physical characteristics of reticulated metal foams

The key physical features of RMFs related to their thermal performance are; the ligament dimensions, surface area, and thermal conductivity. One of the unique advantages of RMFs is that their physical properties can be scaled to provide best solution for a given application. The most effective and practical means of tailoring their characteristics is to apply compression in any combination of 3 orthogonal dimensions. Since the compression can be done at any time after the fabrication of the foam, it provides unique advantages in cost and scheduling of fabricating special and customized applications. The effect of compression on the physical properties is therefore a valuable design information that minimizes the time and the cost of identifying the optimum foam

configuration for any given application. The key features of such structure property relations were reviewed and a set of design equations were provided where possible.

### 3.2.1) Ligament dimensions

An average measure of the ligament dimensions of RMFs can be estimated when the pore density and the relative physical density are given in the as fabricated condition such as 30 ppi and 8% dense. The ligament cross sections are shown in the optical microscope images of various foams in Figures 3 to 8. The microscopy show that the ligament cross sections assume a triangular shape in all foam samples studied. It was assumed that the cross sections of the RMF ligaments are equilateral triangles as defined by the height dimension “d”. Therefore, the relation among the size of a ligament “d”, edge of a dodecahedron “s”, relative density and the pore density of RMF “ $\rho, \alpha$ ”, volume of dodecahedron “ $V_d$ ”, may be estimated by the equation (12) below. The first and the second terms in the equation 12 represent the contributions due to ligaments and nodes, respectively.

$$A_e \cdot (s - \lambda_1 \cdot d) \cdot \frac{\mu_e}{3} + \lambda_2 \frac{\mu_c}{3} d^3 = \rho \cdot V_d \quad (12)$$

where,

$\mu_e = 30$  the number of edges dodecahedron

$\mu_c = 20$  the number of corners of dodecahedron,

$A_e = d^2 / \sqrt{3}$  cross sectional area of a ligament

and,

$\lambda_1$  a linear measure of the nodes

$\lambda_2$  nodal volume shape factor

the numeric values of the  $\lambda$  coefficients were estimated as 1.4 and 0.3, respectively. The ligament size “d” of a number of RMF configurations were obtained from iterative solutions of the equation 12. The calculated (physically meaningful roots) and measured values of ligament dimensions are given in Table 1, The British system of units employed in Table 1 for the sake of compatibility with the commercial definition of the pore density being pore per inch (ppi).

Cell edge “s” (In)	Pore density “ $\alpha$ ” (ppi)	Foam density “ $\rho$ ”	Ligament size “d” calculated (in)	Ligament size “d” measured (in)
0.020	30	0.08	0.0089	0.009
0.027	20	0.08	0.012	0.012
0.040	10	0.08	0.018	0.019

Table 1. Calculated and predicted values of RMF ligament dimensions

The ligament dimension is only a function of the foam density in as fabricated state. Therefore the measured or the calculated ligament size “d” values can be used for compressed foams.

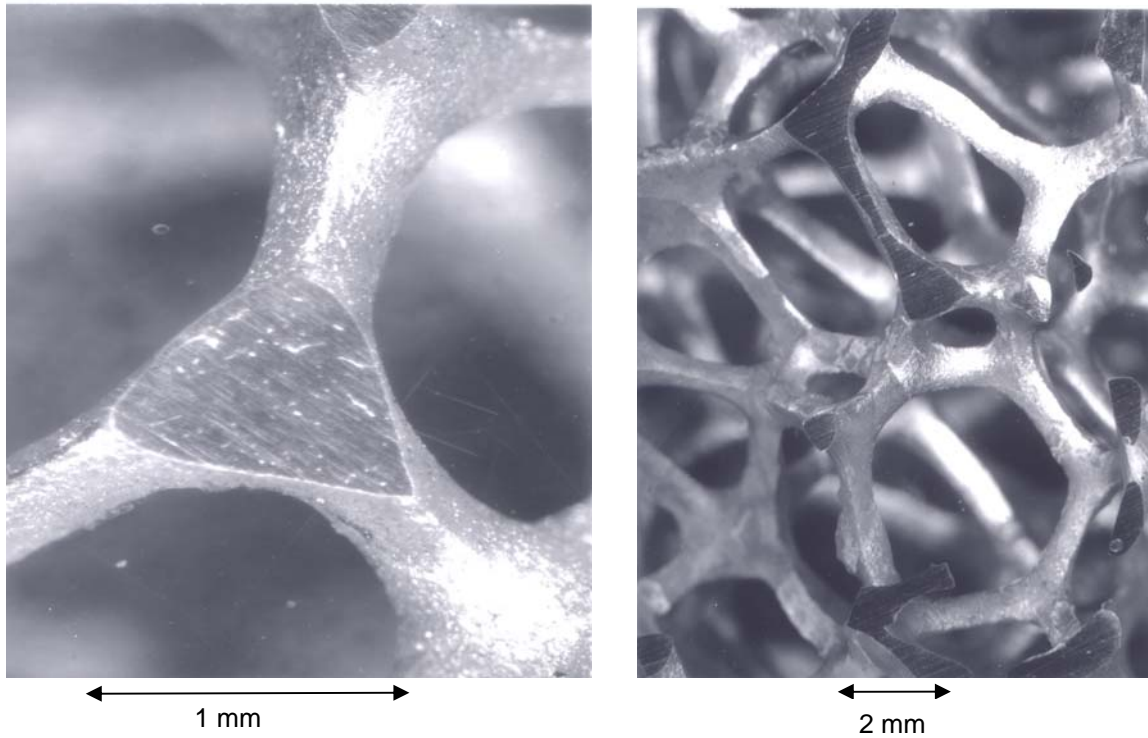


Figure 3. 10 ppi and 8% dense Al foam

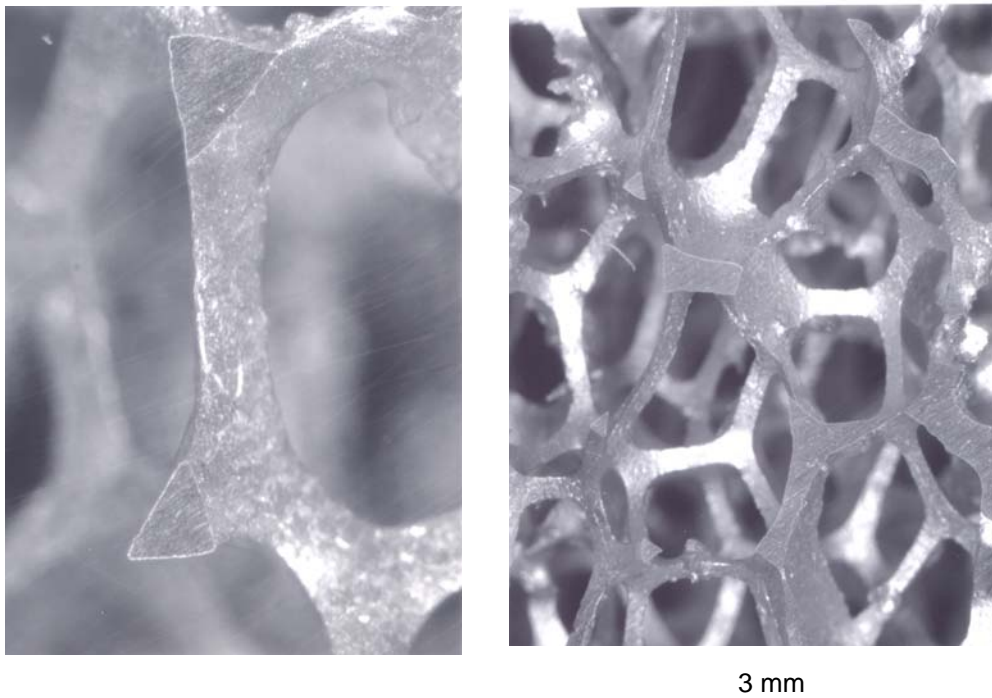




Figure 4. 20 ppi and 8% dense Al foam

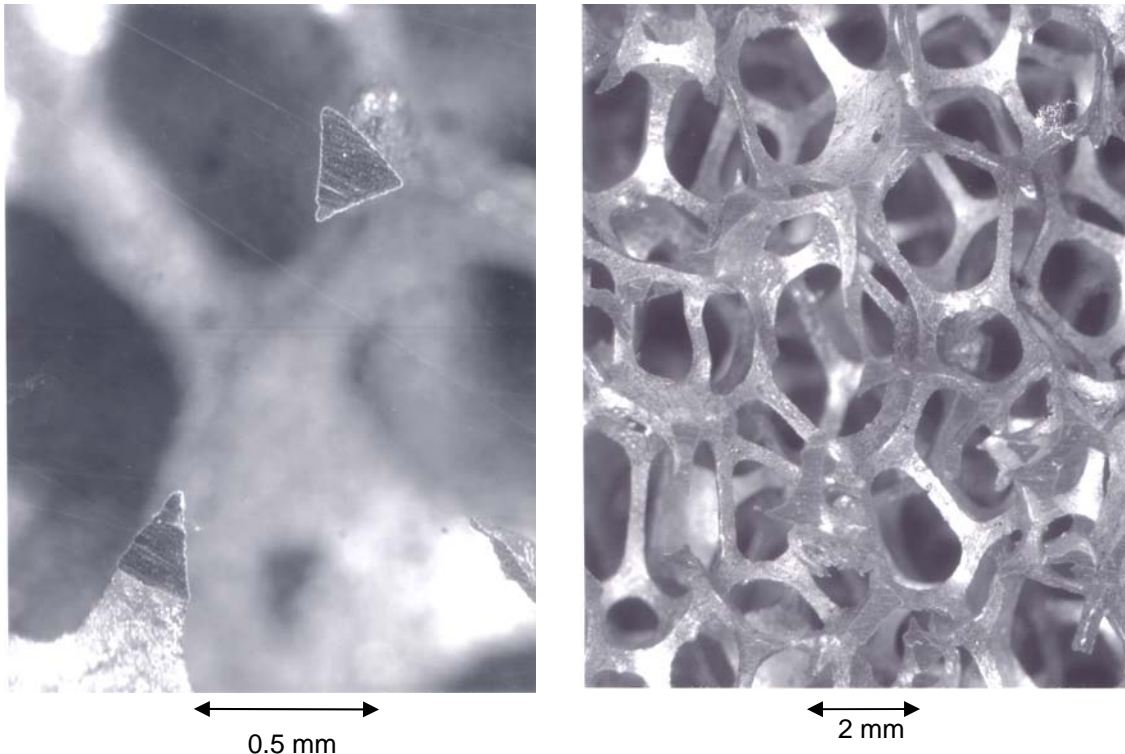


Figure 5. 30 ppi and 8% dense Al foam

### 3.2.2. Surface area density

One of the most important features of the RMFs is their extremely high and scaleable surface area density. The surface area density is directly related to the extended surface area for improved convective heat transfer. The specific surface area or the surface area density of 3 different RMF structures were measured using the multipoint Brunauer, Emmett and Teller (BET) method by adsorption of krypton gas at  $-77.4$  °K [8]. The results of these measurements were compared with the calculated values of the surface densities.

The surface area measurements:

The as manufactured densities of 10, 20 and 30 ppi RMF were measured and the samples were compressed to approximately 30% relative density which increased their surface area and thereby the accuracy of surface area measurements. The surface of the samples effectively cleaned of residual contaminants by the adsorption of krypton at liquid nitrogen temperature and its subsequent desorption during warming back to room temperature. Following the surface cleaning cycle, all samples were outgassed for no less than 48 hours at room temperature under high vacuum ( $\sim 10^{-7}$  torr) prior to measurements. Blank cell measurements were undertaken to account for adsorption of gas on the interior surfaces of the sample cell. The calculated surface area for the blank cell was subtracted from the values for each sample.

The results of the surface area measurements are given in the Table 2 below.

Sample	BET surface area (m <sup>2</sup> /g)	Bulk Density		Density (%)	Specific Surface (m <sup>2</sup> /m <sup>3</sup> )
		(g/ml)	(g/m <sup>3</sup> )		
10 ppi	4.14x10 <sup>-3</sup>	0.217	2.17x10 <sup>5</sup>	8.1	899
20 ppi	7.43x10 <sup>-3</sup>	0.165	1.35x10 <sup>5</sup>	6.1	1266
30 ppi	9.88x10 <sup>-3</sup>	0.145	1.45x10 <sup>5</sup>	5.4	1447

Table 2. Specific surface area of RMFs as measured by BET technique

The specific surface area density  $s_o$  of RMFs may be estimated by equation (13) below, where  $a$ ,  $d$ ,  $\mu_e$ ,  $\mu_c$ ,  $\rho$ , and  $V_d$  has the same meanings as defined in equation (12). It should be noted that  $s_o$  is normalized with relative density  $\rho$  so that it is linearly scaled with % density for the specific RFM.

$$s_o = \frac{d \cdot (a - \lambda_{s1} \cdot d) \mu_e + \lambda_{s2} \cdot d^2 \cdot \frac{\mu_c}{3}}{100 \cdot \rho \cdot V_d} \quad (13)$$

Similarly, the constants  $\lambda_{s1}$  ( $\sim \lambda_1^{2/3} = 1.25$ ) and  $\lambda_{s2}$  ( $\sim \lambda_2^{2/3} = 0.4$ ) are related to surface specific linear measure of the nodes and the nodal surface area shape factor, respectively.

The specific surface area “ $s_o$ ” of the same RMF configurations as the BET samples were obtained from iterative solutions of the equations (12) and (13). The calculated and measured values of  $s_o$  values are compared in Table 3. The results show that the measurements and the calculations are within reasonable agreement.

The specific surface area values for the compressed RMF can be obtained by simply multiplying the  $s_o$  value with the final density in %. It should be noted that the surface area density is a scalar quantity and therefore the compressed value of which is independent of the direction of compression. As a comparison with commercially available alternate materials, the specific surface area values of a pin fin configuration with 1.52 mm diameter pins at 3.05 mm centers, and of a thin fin configuration with 0.76 mm thick fins at 1.52 mm spacing are 11.8 cm<sup>2</sup>/cm<sup>3</sup> and 5.9 cm<sup>2</sup>/cm<sup>3</sup>, respectively.

Sample	Density (%)	Ligament size (m)	Specific surface	
			Measured (in <sup>2</sup> /in <sup>3</sup> /%)	Calculated (in <sup>2</sup> /in <sup>3</sup> /%)
10 ppi	8.1	1.57 10 <sup>-4</sup>	2.8	2.6
20 ppi	6.1	1.06 10 <sup>-4</sup>	5.5	5.1
30 ppi	5.4	7.87 10 <sup>-4</sup>	6.8	7.5

Table 3. measured and calculated surface area density of RMFs.

### 3.2.3. Thermal conductivity

The effective or apparent thermal conductivity is among the key physical properties that is closely related to the thermal performance of RMF based heat exchangers. RMF used for high performance advanced Heat Exchanger (HX) applications are made out of the highest thermal conductivity materials such as Ag, Cu and Al. However, the long length complex shape of the thermal path traveling through the porous media significantly lowers the effective thermal conductivity of the RMF. This observation is particularly relevant to the as manufactured low density (~ 5% to 10%) foams. However, the low density and the open structure of the RMS offers a unique capability to scale and tailor the thermal conductivity of RMF for any given high performance application. This feature allows us to optimize both the cost and the thermal performance of HX for a given application. The high ductility of pure metals allows the RMF to undergo significant inelastic deformation w/o failure of the ligaments. It is also possible to apply intermediate annealing steps to further increase the density of the foam structure up to 50%. Since the thermal conductivity is a vector quantity, its value will be a function of not just the amount of compression (as it is for the effective surface area), but also of the direction of compression.

An experimental and theoretical study was performed to help improve our understanding of the thermal conductivity of RMSs and its relation to the amount of directional compression.

The thermal transport phenomenon in metals involves two distinct physical mechanisms. The first mechanism is the heat conduction through transfer of thermal energy by the free electrons, the same electrons that conduct electricity. The electron gas just like molecular gasses such as N<sub>2</sub>, O<sub>2</sub>, He etc. can conduct heat. The second mechanism of heat conduction is the phonon conductivity or lattice conductivity. The lattice conduction is related to the vibration of atoms due to their thermal energy. Amplitude of lattice vibrations increase at the heated end of a metal and it propogates through the lattice therby transporting the thermal energy. The lattice waves travel at the speed of sound in a given crystal and their propagation can be altered through scattering by alloying and by imperfections. In metals and alloys both of these mechanisms are important. However in pure metals electronic conductivity is large compared with the lattice conductivity. Therefore, good electrical conductors are also good thermal conductors. The law of Wiedemann and Franz [9] states that the thermal conductivity is proprtional to the electrical conductivity and it scales linearly with the absolute temperature, as shown in equation (14).

$$K_{th} = L \cdot K_{el} \cdot T \quad (14)$$

where  $K_t$  and  $K_e$  are the thermal, and the electrical conductivity, respectively.  $T$  represent the absolute temperature, and  $L$  is the Lorenz number ( $2.45 \times 10^{-8}$ ). As an example of its application, calculation of the thermal conductivity of pure Cu at room temperature is shown below.

$$K_{th}(W / m ^\circ K) = 2.45 \cdot 10^{-8} (W \cdot \Omega / ^\circ K^2) * 0.58 \cdot 10^6 (1 / \Omega \cdot m) * 298(^0K)$$

$$K_{th} = 424 \quad (W / m ^\circ K)$$

The thermal conductivity values of RMFs were characterized through electrical conductivity measurements. As discussed above this approach assumes that the lattice contribution of thermal conduction is negligible compared to electron conductivity. A simple approach was used to estimate the thermal conductivity through lattice mechanism to justify the validity of this assumption. Glass ceramics are insulators and their thermal conductivity is mainly due to lattice vibrations. Among the family of crystalline glasses  $\beta$  sodumene ( $Li_2O \cdot Al_2O_3 \cdot 4SiO_2$ ) has the same elastic modulus, the same density and the same grain size as that of Al metal. The modulus and density are the key macroscopic components of lattice vibrations, therefore, the thermal conductivity of  $\beta$  sodumene gives a reasonable estimate of the lattice conductivity in Al. The thermal conductivity of  $\beta$  sodumene is 2 W/m. $^\circ$ K, [9]. Since this is about 1% of the thermal conductivity of Al, it supports our assumption above.

The electrical conductivity of RMF with dodecahedron cell, may be estimated through its structural and bulk physical properties. This approach was taken since it complements the electrical resistance measurements and provides further insight to the thermal conductivity and its dependence to compression. Resistance of a ligament which is shared by three cells in parallel, may be estimated by (15)

$$R_l = \frac{s}{\omega_{cu} \cdot \frac{A_l}{3}} \quad (15)$$

where,  $\omega_{Cu}$  is the bulk conductivity of Cu,  $s$  is the side of dodecahedron and  $A_l$  is the area of the ligament cross section  $\sim \sqrt{3}/4d^2$ . The dodecahedron cell contains 3 such resistance in series and 5 in parallel. The number of such cells in a unit volume "p" is given by  $1/V_d = 1/\beta \cdot s^3$ , where  $\beta = 7.66$  (11). In a unit volume of RMF there are  $p^2$  cells in a layer connected in parallel in a layer, and there are  $p$  such layers connected in series. Therefore the equivalent resistance of a unit volume is given by  $R_e$ .

$$R_e = \frac{1}{\omega_e} \approx \zeta \frac{1}{\omega_{cu}} \cdot \left(\frac{s}{d}\right)^2 \quad (16)$$

where,

$$\zeta = 4 \cdot \sqrt{3} \cdot \beta^{1/3} \cdot (3/5) \quad (17)$$

and

$$(d/s)^2 \approx \left(\frac{3\sqrt{4}\beta}{\mu_e}\right) \cdot \rho \quad (18)$$

Combining (16) and (18)

$$\omega_e = \lambda \cdot \omega_{Cu} \cdot \rho \quad (19)$$

$$k_e = \lambda \cdot k_{Cu} \cdot \rho \quad (20)$$

where the numerical value of the proportionality constant  $\lambda = 0.346$ . Since the thermal and electrical conduction are physically similar phenomenon, the same equation (19) would hold for thermal conductivity as well.

Experimentally, 30 ppi and 10 ppi RMF samples were attached to current terminals, by eutectic Pb/Sn solder in inert environment, Figure (6). A Sorenson DC power supply was used to apply 30 Amp current in the current control mode. The current leads of the power supply was screw attached to the current terminals. The temperature of the sample was monitored with K type thermocouple wires during the test. Thermocouple wires were bonded to the foam sample at three different locations by thermally conductive electrically insulating AlN filled epoxy. The thermocouple location were at the center of the sample (1) and about 1 cm away from the current leads (2)

The DC voltage across the Cu foam pieces was measured with an HP 34401A digital multimeter using kelvin probes with  $10\mu V$  accuracy . Electrical resistance measurements were repeated after every compression cycle. At the end of each test samples were desoldered from the terminals, and moved to the pressing station. The boundary displacements for inducing compressive inelastic strains in any given material direction were applied by means of a mechanical press and their magnitude was measured with a micrometer. The weight and the dimensions of samples were measured before they were soldered to the current terminals for testing.

The initial dimensions of the nominal 30 ppi and 10 ppi RMF samples were 1.9 cm x 1.9 cm x 12.7 cm and 5.04 cm x 5.04 cm x 12.7 cm respectively. The magnitude of compression applied in x,y and z directions of the 20 ppi sample were 0.44, 0.46 and 0.3, respectively. The uniformity of the deformations were verified by optical microscopy on the sample surfaces. No significant variation was noticed in the cell dimensions along the axis of compression. The results of the compression experiments are summarized in the Table 4 below.

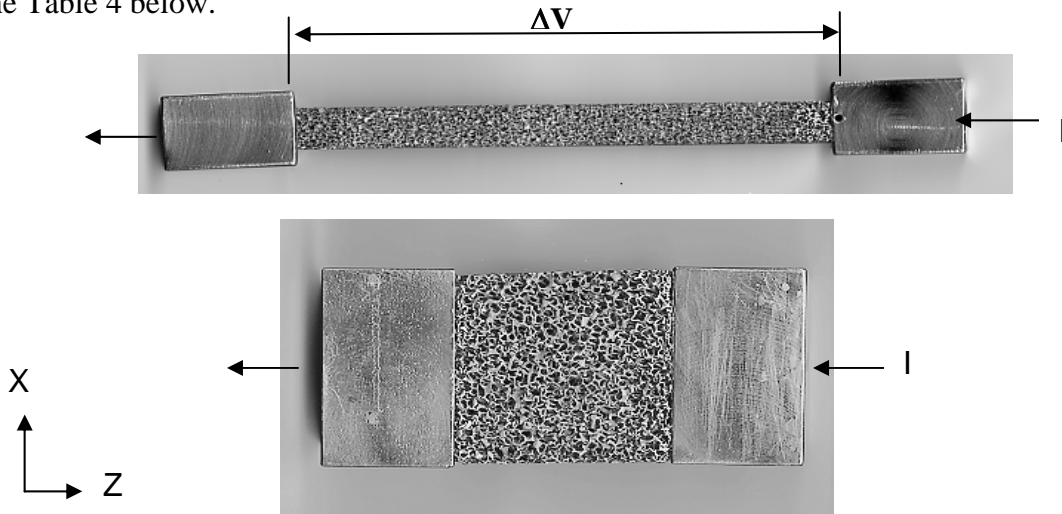


Figure 6. Cu RMF test samples for electrical resistance measurements soldered to current terminals. The Cu current blocks have the same cross sectional area as that of the as received samples.

The thermal and electrical bulk conductivity of Cu was taken as 400 (W/m-°K) and  $0.593 \times 10^6$  (1/Ω-cm), respectively.

Run # ppi	L (cm)	Area (cm <sup>2</sup> )	Density (ρ)	ΔL/L	I (Amp)	ΔV (Volt)	$\omega_e/\omega_{Cu-\rho}$ (λ)	$K_{eff}$ (W/m-°K)
1-30	1.97	0.295x0.295	0.088	0	30	5.8x10 <sup>-3</sup>	0.3575	12.2- x,y,z
2-30	1.97	0.305x0.165	0.151	-0.436, y	30	5.9x10 <sup>-3</sup>	0.3420	20.6- x,z
								7.2- y
3-30	1.97	0.169x0.165	0.272	-0.457, x	30	5.9x10 <sup>-3</sup>	0.3457	37.2- z
								11.4- x
								13.0- y
4-30	1.38	0.173x0.165	0.391	-0.300, z	30	5.9x10 <sup>-3</sup>	0.3475	26.0- z
								16.4- x
								18.7- y
1-10	1.85	0.787x0.787	0.083	0	30	0.81x10 <sup>-3</sup>	0.3571	11.6- x,y,z
2-10	1.05	0.811x0.811	0.136	-0.432, z	30	0.75x10 <sup>-3</sup>	0.3420	7.08- z
								19.0- x,y

Table 4. Results of electrical resistance measurements on 30 ppi and 10 ppi RMF

The results of electrical resistance measurements and thermal conductivity calculations show that both the thermal and electrical conductivity are inversely or directly proportional to the increase in foam density i.e.  $1/(1+\epsilon_p)$ , depending on the direction of compression applied. These properties are reduced in the the direction of compression but isotropically increased in the plane perpendicular to the direction of compression. The compression increase the thermal or electrical resistance by increasing the number of resistive elements that are in series in the direction of compression. It reduces the thermal or electrical resistance by increasing the number of resistive elements that are in parallel in the perpendicular directions to densification. It should be noted that regardless of the direction, compression always increases the actual density.

### 3.2.4 Convective energy transfer.

The local convective energy transfer rates or the local film coefficients have a significant effect in overall thermal transfer performance of RMF based HXs. RMF provides flow passages with small hydraulic diameter which is inversely proportional to the convective conductance  $h$ . A measure of hydraulic diameter is related to the pore density, ligament size, and the relative density of the foam. Although, the as-fabricated value of the

relative density is usually  $< 10\%$ , it can be increased, by the way of compression to up to  $50\%$ . From point of view of designing and fabricating prototype HX, compressibility in the bulk form scales the thermal performance of the foam allows us tailor the material for any given application. As a result, the development cycles shortened, and the cost and the time to market indices are significantly improved.

The local convective heat transfer of a RMF based HX can be improved by reducing the hydraulic diameter and the ligament dimension. As the ligament size reduced so is the thickness of the local boundary layer which improves the local convection conduction. Since reducing the ligament dimension also increases the surface area factor, the thermal performance is further enhanced. On the other hand, compression increases the material cost, and both the reduction in ligament length and the compression increase the friction factor. The cost, the thermal performance and the flow resistance are coupled, and therefore, an optimum HX design must considers all three factors. The following relationships help understand the coupling among these factors.

$$l \approx (\rho/\eta)^{-p} \frac{1}{\alpha} - d \quad (21)$$

$$D_h \approx 2 \cdot \frac{l_1 \cdot l}{l_1 + l} \quad (22)$$

$$\omega_1 \approx l_1 \cdot l \cdot \alpha_1 \cdot \alpha \quad (23)$$

where;

$p=0, 0.5$  or  $1$  for as fabricated, biaxially compressed and uniaxially compressed foams, respectively.  $\rho$  and  $\eta$  are the as fabricated and compressed density of foam, and  $\alpha$  and  $d$  are the as fabricated pore density (ppi) and ligament diameter of foam, respectively.  $l$  and  $l_1$  are the as fabricated and the compressed cell sizes, respectively.  $D_h$  is a measure of the hydraulic diameter. If the heat flux is perpendicular to  $xy$  plane, then  $l$  and  $l_1$  may be reviewed as  $l_z$  and  $l_x$  or  $l_z$  and  $l_y$ , depending on the direction of flow being in the  $y$  or  $x$  direction, respectively.  $\omega_1$  is a measure of the constrained flow area, and  $1/\alpha_1=(l_1+d)$  by definition.

In case of the compressed foams, the directional coupling needs to be included in the effective  $D_h$  and  $\omega$  calculations. It has been observed that the effect of compression in one direction effects the hydraulic diameter and the constrained flow area measurements in the perpendicular directions as well. In another words compression say, in  $x$  direction effects flow resistance in the  $y$  and  $z$  direction. Experimental observations suggest that a set of estimates of the coupling coefficients that support the test data reasonably well are  $0.6$  and  $0.4$  for  $c_1$  and  $c_o$ , respectively. Therefore,

$$D_{he} = (c_1 \cdot D_o + c_o D_1) \quad (24)$$

$$\omega_{he} = (c_1 \cdot \omega_o + c_o \omega_1) \quad (25)$$

where indices 0 and 1 refer to as fabricated and compressed states. For example, if the flow direction  $x$  is parallel to the direction of compression then the effective value of the hydraulic diameter is  $0.6D_0 + 0.4D_1$  where  $D_0$  and  $D_1$  refer to the as-fabricated and compressed values. Since the surface perpendicular to the flow direction is not compressed, as-fabricated values of  $D$  or  $\omega$  dominate, see Figure 7 and Figure 8.

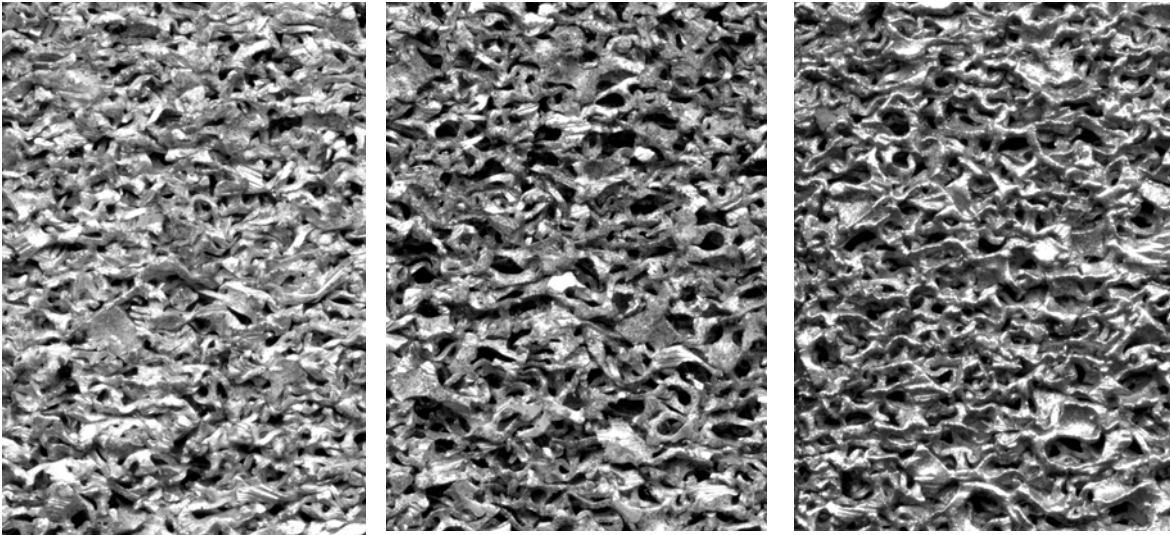


Figure 7. 30 ppi foam uniaxially compressed to 35% density in plane (left) and out off plane (middle), 30 ppi foam biaxially compressed to 35% density (right)

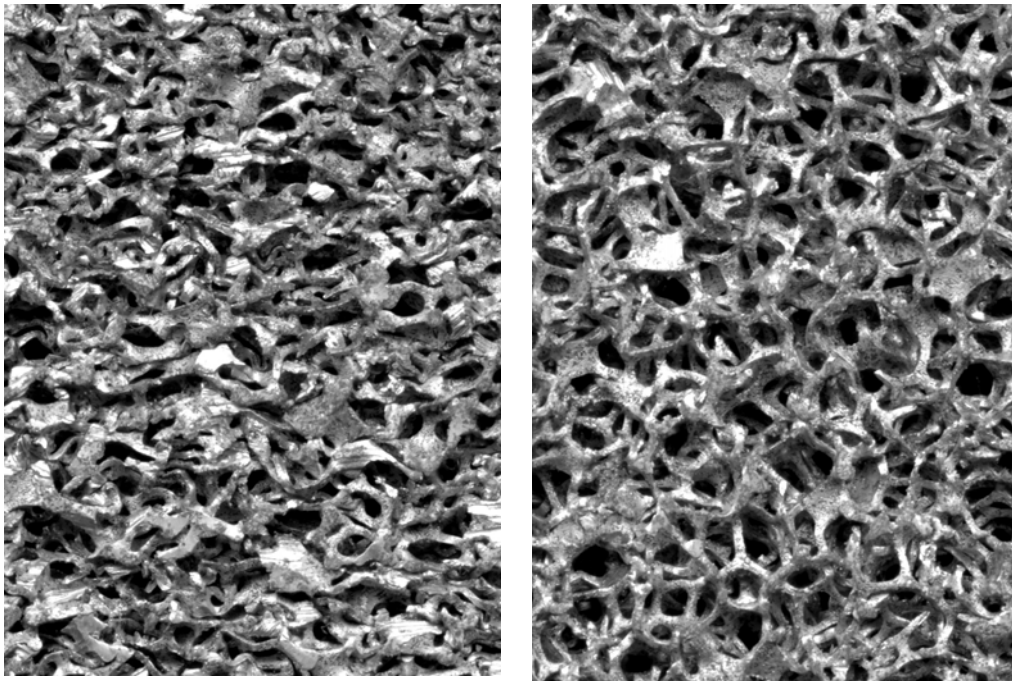


Figure 8. 30 ppi foam uniaxially compressed to 20 % density in plane (left) and out off plane (right).

The value of the local convective conduction is a function of the fluid properties, flow properties and the characteristics of the RMF. Due to the complex geometry and flow conditions, the local  $h$  factor can not be expressed in closed form equations. However, it may be calculated by numerical techniques such as Computational Fluid Dynamics (CFD) or it may be measured experimentally. Such a study will not be presented here but it will be reported in a future publication.

#### 4.0 Thermal Performance Limits for RMFs

The maximum thermal performance of RMF based HX is an important factor in the selection of HX technology. The thermal performance limits of RMF HX will be estimated for both water and air cooled applications. The effective  $h$  factor, the coolant, the foam density and the foam thickness will be tabulated and presented in terms of 3D surface plots. In order to proceed with such calculations we will assume that the value of the local  $h$  factor is the highest one reported in experimental studies. The highest local  $h$  values reported for forced convection conditions with water and air are about 0.01 and 1  $W/cm^2\text{-}^\circ C$ , respectively [10].

The pore density  $\alpha$ , the relative density  $\rho$ , the thickness of foam, and the physical properties of coolant are among the key design variables that will strongly influence the maximum thermal performance of foam based heat exchangers. The Ozmat Model [11] assumes that the heat transfer is one dimensional and the heat flux from a thermal base of unit area is uniform and it diminishes at the opposite end of the foam. Since a detailed description of the model is given elsewhere [11], only the results of the study will be presented here.

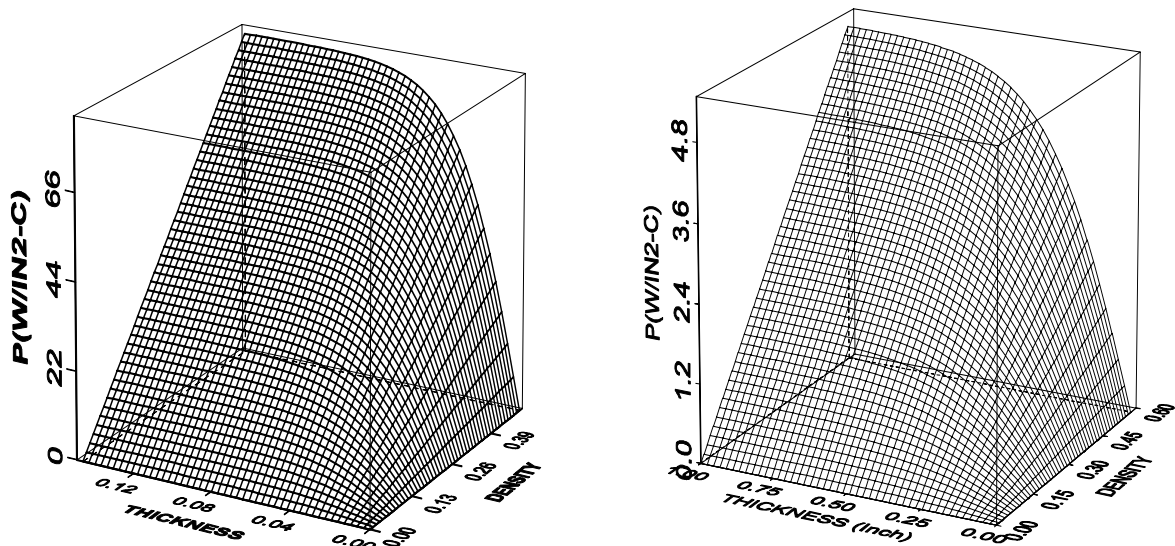


Figure 9. Thermal performance of 30 ppi Cu RMF, water as the coolant (left) and air as the coolant (right)

The predictions of the model are shown below (Figure 9) for 30 ppi foams as a function of the volumetric density and the thickness of foam. The vertical axis shows the value of

the heat flux from a unit base area for a unit temperature difference between the base and the coolant, i.e. the effective convective conduction,  $h_{eff}$ . The results of the calculations for Cu based 30 ppi RMF HX for both water and air are shown below as 3D surface plots in Figure 9. Table 4 summarizes the results for 10, 20 and 30 ppi foam based HXs using both air and water as coolants.

The results show that the effective thickness of foam strongly depend on the film coefficient attainable with a specific coolant. As a comparison with commercially available alternative technology using an external cold plate commonly employed by main frame computer manufacturers, RMF base integral HX may improve the external thermal resistance by an order of magnitude ( $0.14 \text{ } ^\circ\text{C}/\text{W-in}^2$  vs.  $0.015^\circ\text{C}/\text{W-in}^2$ ).

The results of this study show that the RMF heat exchangers may have effective convective conduction coefficients increased by about a factor of 40 as compared to the highest numbers measured for local film coefficients. It is also noted that the critical thickness values for air based HXs is about an order of magnitude larger than that of liquid based HXs. The thermal performance becomes a linear function of relative density when the thickness exceeds the critical value. It is also observed that the thermal conductivity of the foam material has a significant effect on both the thermal performance and the critical thickness.

FOAM MATERIAL	PORE DENSITY (PPI)	CRITICAL THICKNESS (cm)	COOLANT	$Q_{max}/\Delta T-A$ ( $\text{W}/^\circ\text{C}-\text{cm}^2$ )	$R_{th}$ ( $^\circ\text{C}/\text{W}$ )
Cu	10	0.229	WATER	4.65	0.22
Cu	20	0.152	WATER	6.98	0.14
Cu	30	0.114	WATER	10.08	0.10
Cu	10	2.159	AIR	0.43	2.30
Cu	20	1.321	AIR	0.78	1.29
Cu	30	1.016	AIR	1.09	0.92
Al	10	0.178	WATER	3.57	0.28
Al	20	0.127	WATER	5.12	0.20
Al	30	0.076	WATER	7.75	0.13
Al	10	1.905	AIR	0.31	3.23
Al	20	1.016	AIR	0.54	1.84
Al	30	0.965	AIR	0.78	1.29

Table 5. Thermal performance limits and the critical thickness values

## 5.0 Structural compliance of RMF

A somewhat qualitative and cursory review of the basic elements of the mechanical properties of RMF structure is presented below. The purpose of this section is to point out to a rather unique feature of the RMFs that allows us to built integral HXs with a broad range of materials. A more rigorous and quantitative treatment of the subject will be presented in an upcoming publication.

The compliance of RMF depends on the linear elastic, non-linear elastic and non linear plastic characteristics. The elastic modulus of the foam,  $E_f$  is controlled by the bending of the ligaments and it is related to the theoretical density of the foam by the following relationship [12].

$$\frac{E_f}{E_s} = C \cdot \rho^2 \quad (26)$$

Where, s refers to the modulus (E) and the density ( $\rho$ ) of the solid material, and C is a known constant the value of which is about 1. The maximum stress on the stress strain curve is bounded by the elastic buckling of the ligaments. Once the elastic collapse takes place, the maximum stress is limited to about 5% of the apparent modulus (~3.5 MPa) which further reduces the effective modulus of the material. The foam may also collapse by plastic deformation. When the plastic moment of the cell ligament is exceeded, plastic hinges develop causing large deformations at practically a constant level of stress. The plastic collapse stress of a 10% dense material is about 1% of the yield stress of the solid material (~0.35 MPa for 1100 Al). Both the elastic and the plastic collapse of the foam structure reduce the effective modulus and limits the maximum stresses that foam can support. In addition to the low effective modulus, the effective dimension of the bond area between the RMF and the low expansion substrate may be arbitrarily reduced to further lower the interface stresses so that thermal cycle related reliability requirements of any given application could be met. This is accomplished by slicing the monolithic RMF to a set of smaller pieces like a jig saw puzzle with square or rectangular pieces by using a thin blade of diamond saw or wire EDM. These pieces would then be fixtured prior to the bonding process. In case of a plastically deforming interface the maximum size of the puzzle pieces may be estimated by using equation (27).

$$L = \chi \frac{2 \cdot h \cdot \gamma}{\Delta \alpha \cdot \Delta T} \quad (27)$$

Where, L is the maximum size of RMF,  $\Delta \alpha$  is the CTE mismatch between the RMF and the base substrate,  $\Delta T$  is the temperature difference, h is the thickness of the bond layer, and  $\gamma$  is the maximum allowable shear strain, and  $\chi$  is a material constant related to plastic modulus and the thickness of the bond layer and the RMF. For Cu foam, a high temp solder such as 90/10 Pb/Sn bond material, and AlN base material, typical values of the variables are:  $\chi = 2$ ,  $\Delta \alpha = 14E-06$ ,  $\Delta T = 75$  °C,  $h = 0.005$ ”,  $\gamma < 2\%$  and  $L = 0.400$ ”.

The reticulated metal foam structure has a very high effective compliance that allows us to hard bond the foam by soldering or brazing to low CTE material. Since the CTE mismatch related thermal stresses and deformations are limited, the reliability of the integral heat exchanger, and the thermal base ( usually a metalized ceramic plate carrying

directly attached semiconductor devices) is not compromised as verified by hundreds of thermal cycles [13].

### 5.0 An experimental study of RMF based HX

Due to its high thermal conductivity, compatibility with DI water, and solderability to copper metalized surfaces, Cu102 based RMF was selected for the experimental study as the integral compact heat exchanger material. To improve the thermal conductivity and the specific surface area Cu foam was biaxially compressed from as fabricated 8% relative density to 35% relative density, Figure 10.

A block of 30 ppi, 35% dense Cu foam was cut 5.08 cm x 3.3 cm x 0.825 cm dimensions and subsequently it was sliced to 5 rectangular pieces along the 3.3 cm long edge. A 0.0102 cm thick AlN thermal base plate was metalized on both sides with active brazed 0.00127 cm thick Cu. The bottom side Cu metalization is patterned by chemical etching. The Cu foam and the metalized AlN plate were bonded together with 10Sn90Pb high temperature solder in an inert atmosphere. It was observed on the bonded assembly that thermal displacements (bowing ~ 0.0051cm /5.588 cm) at room temperature were not significant, (Figure 11.)

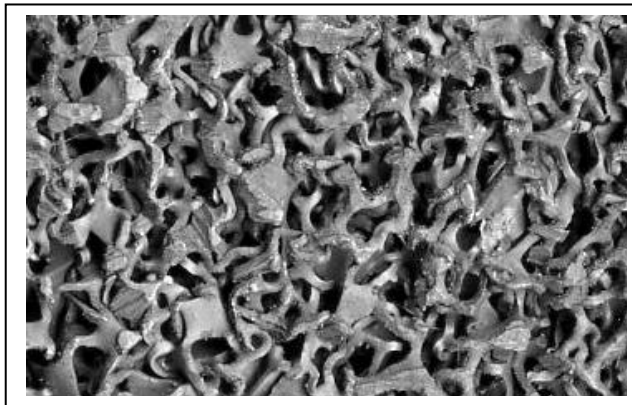


Figure 10. A 30 ppi, 8% dense Cu foam was biaxially compressed to 35% density.

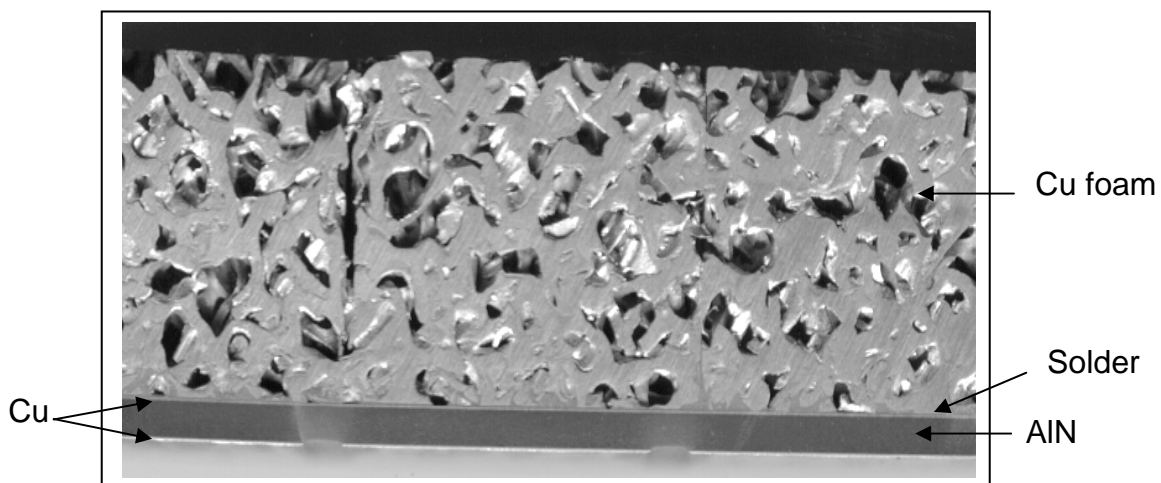


Figure 11. A Cu foam based integral heat exchanger

Experimentally, to verify the performance of foam based heat exchangers a thermal test module was designed and built. The test module employed (4) lidded power devices in series as a set of variable resistors, Figure 12 (a). The dissipation of each Integrated Gate Bipolar Transistor (IGBT) device was independently varied by changing their gate voltage. The temperature of each power device was monitored by using thermocouples attached to their lid metalization. During a typical test, the power dissipation in each resistor, the temperature of each resistor, flow rate and the flow resistance, and the inlet and outlet temperatures of the coolant were monitored. A series of tests were run at 1000W power dissipation and at varying flow rates. The results of these tests are shown in Figure 13, and listed in Table 7.

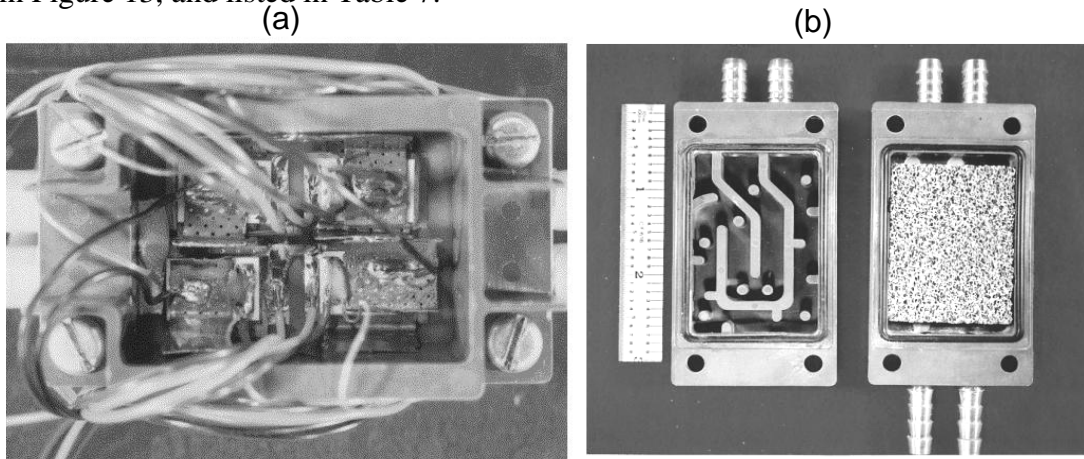


Figure 12. Thermal test module with (4) IGBT resistors in series (a), External HX housing and integral RMF HX housing (Cu foam is separated from AlN base) (b)

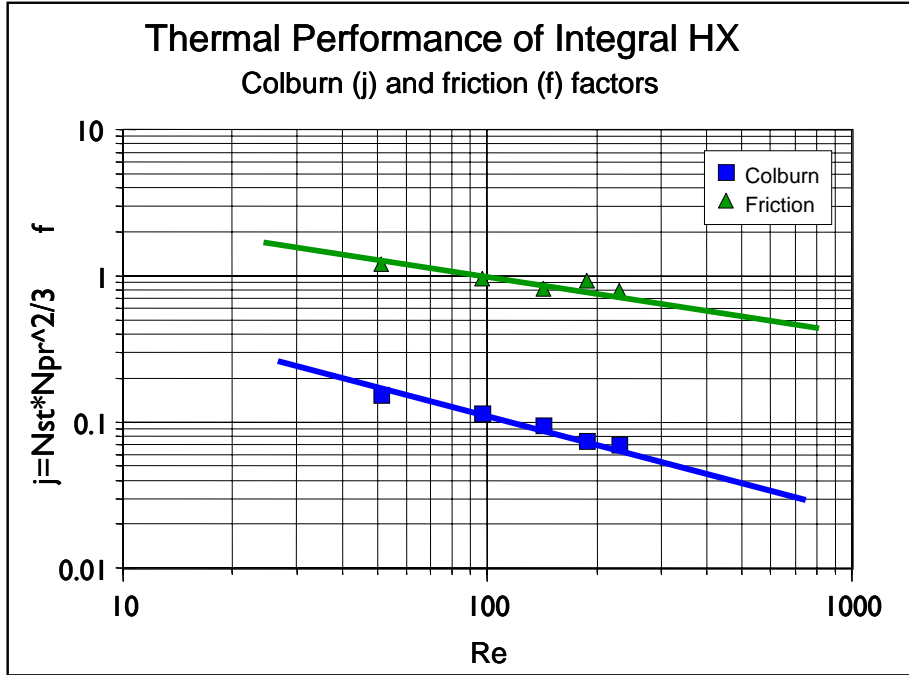


Figure 13. The heat transfer and flow friction data for 40 ppi, 40% dense Cu foam based integral heat exchangers.

In addition to the experimental study, a 3 dimensional FEA was also performed to predict the results of the second set of experiments as shown in Table 5 below. The FEA used the effective  $h$  factor as predicted by the first set of experiments, Figure 20. It was assumed that the heat was uniformly generated in the top 0.0102 cm thickness of the 0.0406 cm thick power devices where the active area of the power device is 1 square cm. The thickness and the conductivities of materials in the test module stack are shown in the Table 6. The solder layer S3 refers to the 90/10 Pb/Sn high temperature solder used in the foam attachment, and the other solder layers refer to the same eutectic Pb/Sn solder. It was assumed that the heat is removed by forced convection to the coolant water running at 0°C temperature. The total dissipation level was taken as 800W per test module, and 200 W per resistor. The effective  $h$  value of 40 W/in<sup>2</sup>-°C was used at the water flow rate of 2 GPM. Figures 14 and 15 show the FEM with gray scale coded for materials and the temperature distribution in the test model as predicted by FEM, respectively. The FEA simulated the experiment number 7 as shown in the Table 6. The results of the test and the analysis are in excellent agreement. The pressure drop at the specified flow rate was less than 69 KPa psig for 4.57 cm long flow length and 0.89 cm x 3.3 cm flow area.

It is noted that the experimental results were obtained from the thermal test modules with 20.64 cm<sup>2</sup> base area, and with for 4 power devices as variable resistors. The total area of dissipation for all for resistors is approximately 6.45 cm<sup>2</sup>. Therefore, the tabulated thermal resistance values for the integral RMF based heat exchangers need to be scaled with a factor of 3.2 to estimate the performance limits on the test module configuration.

Material layers	t (inch)	$K_{th}$ (W/cm-°C)
Cu electrodes	0.010	3.900
Solder (S1, S2, S4)	0.002	0.400
Solder (S3)	0.002	0.300
Lid metalization (Al)	0.002	1.800
Lid (Al <sub>2</sub> O <sub>3</sub> )	0.025	0.300
Silicon	0.016	0.800
Thermal base (AlN)	0.040	2.700

Table 6. Thickness and thermal conductivity of the materials

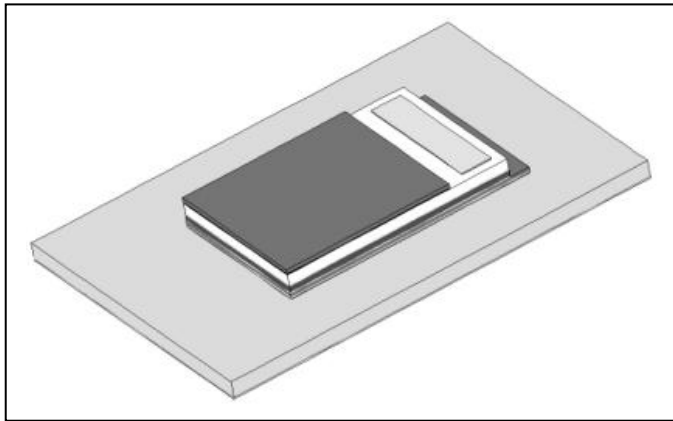


Figure 14. FEM of the thermal test module gray scale coded for materials.

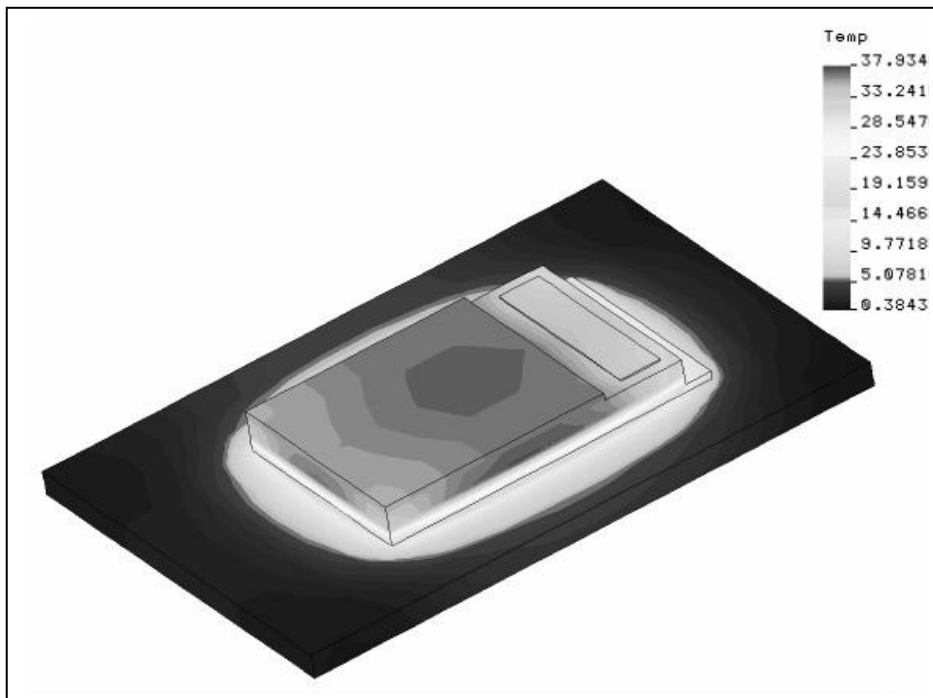


Figure 15. Temperature distribution in the test module

	Heat Sink	$\Delta T_{ja}$ , (°C)	R <sub>ja</sub> (°C/W)	P <sub>max.</sub> @ $\Delta T_{ja}$ 60 °C
1-FEM	INTEGRAL-30 ppi Cu-36 %	60	0.043	1,400
2	BAFFLED CAVITY	75 °C @ 800W	0.095	640
3	EXTERNAL Cold Plate	95 °C @ 800W	0.120	505
4	INTEGRAL-30 ppi Al-10%	86 °C @ 800W	0.108	560
5	INTEGRAL-30 ppi Al-20%	69 °C @ 850W	0.080	740
6	INTEGRAL-30 ppi Al-36%	47 °C @ 850W	0.059	1020
7	INTEGRAL-30 ppi Cu-36 %	38 °C @ 800W	0.047	1310
8	INTEGRAL-30ppi Cu-36 %	63 °C @ 1000W <sup>E/G</sup>	0.063	950
9	INTEGRAL-30ppi Cu-36 %	35 °C @ 500W <sup>EO</sup>	0.070	860

E/G: 50% Water-Ethylene Glycol mixture  
EO : Engine Oil, Castrol 399.

Table 7. Results of the FEA and the second set of tests

The thermal performance limit calculations assume that a uniform heat flux is applied over the entire 6.54 cm<sup>2</sup> base area. The ratio of the entire base area over the area of heat flux is 3.2. In summary, the thermal performance of advanced power modules may be improved by a factor of 2, if a high performance integral heat exchanger is incorporated in to the design. The low cost, low weight and reduced size requirements for advanced power module systems may be more readily achieved by integral heat exchangers than external cold plates and heat spreaders.

## 6.0 Conclusions

The analytical and experimental studies were performed to characterize the thermal and related structural properties of RMF based heat exchangers. It was shown that increasing the as fabricated specific density of the foam by successive compression and annealing steps is one of the key features of the RMF based HX technology. The compression increases the specific surface area, the local convective heat transfer, the effective thermal conductivity in the direction perpendicular to the plane of compression, and the flow resistance of RMF matrix. Selecting the amount and the direction of compression as well as the initial pore size and relative density allow us tailor the properties of RMF for a given application

In summary, the current study illustrated that the RMF based heat exchangers offer significant advantages over the alternative current approaches to compact heat exchangers. Among those advantages the most note worthy ones are:

- a) Large specific surface area
- b) Superior and scalable thermal performance

- c) Low weight and volume
- d) Compatibility with a large range of coolants
- e) High structural compliance and specific stiffness.
- f) Hard bondability to low expansion substrates.

These advantages (6) and the constitutive properties of densified RMF matrix are the basis of performance, cost and reliability of RMF based integral HXs.

It is also recommended that, among those properties, the inelastic constitutive (mechanical) behavior of RMF should be more thoroughly studied both experimentally and theoretically.

## REFERENCES

- [1] D. Mundinger et al, "High Average Power Edge Emitting Laser Diode Arrays on Silicon Microchannel coolers," *Apply Physics Letters*, V 57, no 21, 1990.
- [2] L. J.Missaggia et al, Micro Channel heat Sinks for two-Dimensional High-Power-Density Diode Laser Arrays," *IEEE J. Quantum Electronics*, V 25, no.21, 1989
- [3] Mahajan, R. L., Arbelaez, F. and Sett, S.,(2000), "An experimental study on pool boiling of saturated FC-72 in highly porous aluminum metal foams", Paper # NHTC 2000-12192, Proceedings 34th National Heat Transfer Conference, Pittsburgh, PA, Aug. 20-22, .
- [4] Sorgo M., "Thermal Interface Materials," *Electronics Cooling*, Vol. 2, No. 3, pp. 12 -16., Sept. 1996.
- [5] Calamidi, V.,V. "Transport Phenomenon in High Porosity Fibrous Metal Foams", University of Colorado, Department of Mechanical Engineering, PhD Thesis, 1997.

- [6] Bastawros and Evans, A., G. "Characterization of Open-Cell Aluminum Alloy Foams as Heat Sinks for High Power Electronic Devices" Symposium on the application of Heat Transfer in Microelectronics Packaging, IMECE, 1977.
- [7] Leyda B., ERG Technical Reports "Engineering Properties of DUOCEL Reticulated Metal Foams" 900 Stanford Avenue, Oakland CA 94608
- [8] Brunauer, Emmet, Teller, Journal of the American Chemical Society, Volume 60, 1938, p 309.
- [9] Wiedemann and Franz, Proc. Phys. Soc. 77 (1 May 1961) 1005-1013
- [10] McMillan, P., W. "Glass-Ceramics, Academic Press, 1979
- [10] Malingham, M. "Thermal Management in Semiconductor Device Packaging" Proceedings of IEEE, V.72 No. 9, 1985
- [11] Ozmat B., et al. "An Advanced Power Module Technology for High Performance Devices and Applications" Proceedings of PCIM 1998.
- [12] Ashby M. F., Medalist R. F. M., 1983 "The Mechanical Properties of Cellular Solids" Metallurgical Transactions A, Volume 14A, September 1983, pp. 1755-1786.
- [13] Final Program Report, COMNAVSEASYS COM contract N00024-94-NR58001.